01 Jul 2014

Probing Long-Range Intensity Correlations inside Disordered Photonic Nanostructures

Raktim Sarma

Alexey Yamilov
Missouri University of Science and Technology, yamilov@mst.edu

Pauf Neupane

Boris Shapiro

et. al. For a complete list of authors, see https://scholarsmine.mst.edu/phys_facwork/1027

Recommended Citation

R. Sarma et al., "Probing Long-Range Intensity Correlations inside Disordered Photonic Nanostructures," *Physical review B: Condensed matter and materials physics*, vol. 90, no. 1, pp. 014203-1-014203-5, American Physical Society (APS), Jul 2014.
The definitive version is available at https://doi.org/10.1103/PhysRevB.90.014203

Probing long-range intensity correlations inside disordered photonic nanostructures

Raktim Sarma,[1] Alexey Yamilov,[2,*] Pauf Neupane,[2] Boris Shapiro,[3] and Hui Cao[1,†]
[1]*Department of Applied Physics, Yale University, New Haven, Connecticut 06520, USA*
[2]*Department of Physics, Missouri University of Science and Technology, Rolla, Missouri 65409, USA*
[3]*Department of Physics, Technion-Israel Institute of Technology, Haifa 32000, Israel*
(Received 24 May 2014; revised manuscript received 2 July 2014; published 21 July 2014)

We report the direct observation of the development of long-range spatial intensity correlation and the growth of intensity fluctuations inside random media. We fabricated quasi-two-dimensional disordered photonic structures and probed light transport from a third dimension. Good agreement between experiment and theory is obtained. We were able to manipulate the long-range intensity correlation and intensity fluctuations inside the disordered waveguides by simply varying the waveguide geometry.

DOI: 10.1103/PhysRevB.90.014203 PACS number(s): 71.55.Jv, 42.25.Bs, 72.15.Rn

I. INTRODUCTION

Light propagation in disordered media has been a topic of intense studies for nearly three decades [1–3]. In analogy with electronic transport in disordered metals, fundamental issues related to diffusion and localization have been addressed [4,5]. One interesting example is long-range intensity correlation [6], which characterizes mesoscopic transport of both classical and quantum waves, and reflects the closeness to the Anderson localization threshold [7]. Experimentally, correlations in time, space, frequency, angle, and polarization have been investigated, but most measurements are performed on transmitted or reflected light outside the random media [8–16]. It would be interesting to probe correlation inside the random media and to monitor how long-range correlation builds up as light propagates through the random medium. However, it is very difficult to probe transport inside three-dimensional (3D) random media. Only in a microwave experiment was a detector (antenna) inserted into the random media to measure the intensity inside [8]. Alternatively we design and fabricate quasi-two-dimensional (2D) disordered waveguides to probe light transport inside from the third dimension [17]. This approach will allow us to directly measure intensity correlation and fluctuations inside random structures. Furthermore, we vary the degree of long-range intensity correlation by changing the waveguide geometry.

The intensity-intensity correlation function C consists of three terms, short-range C_1, long-range C_2, and an infinite-range C_3 correlation. Intuitively, interferences between waves scattered along independent paths give rise to C_1, one crossing of paths generates C_2, and two crossings cause C_3 [18,19]. The spatial correlation term C_1 decays exponentially with increasing distance and vanishes beyond the transport mean free path ℓ. C_2 also decays but much more slowly, while C_3 has a constant contribution. The long-range correlation dominates fluctuations of total transmission $T_a \equiv \sum_b T_{ab}$, where T_{ab} is the transmission from an incoming wave mode a to an outgoing mode b. The magnitude of C_2 is on the order of $1/g$, and C_3 of $1/g^2$, where $g \equiv \sum_a T_a$ is the conductance [12,20]. When $g \gg 1$, C is dominated by C_1. To measure C_2, the spatial distance must exceed the transport mean free path so that C_1 dies out. Alternatively, C_2 can be measured by collecting all transmitted light using an integrating sphere. This method, however, cannot be used to measure C_2 *inside* the sample. Instead, we integrate light intensity over the waveguide cross section to average out the short-range fluctuation, and directly measure the long-range correlation inside the disordered *planar waveguide*. The conductance of the waveguide is $g = (\pi/2)N\ell/L$, where $N = 2W/(\lambda/n_e)$ is the number of propagating modes in the waveguide. L is the waveguide length, W is the waveguide width, λ is the light wavelength in vacuum, and n_e is the effective index of refraction of the random medium [21]. Hence, by decreasing W, we are able to reduce g and enhance the magnitude of C_2 without modifying the structural disorder.

This paper is organized as follows. In Sec. II, we describe the design and fabrication of 2D disordered waveguides as well as the optical measurement of intensity correlation inside the waveguide. Section III contains the calculation of long-range correlation inside the disordered waveguides and the formula for the physical quantities that are measured experimentally. Section IV presents the experimental data and comparison to the theory. Finally we conclude in Sec. V.

II. 2D DISORDERED PHOTONIC STRUCTURES

The 2D disordered waveguides were fabricated in a silicon-on-insulator (SOI) wafer with a 220 nm silicon layer on top of a 3 μm buried oxide (Fig. 1). The patterns were written by electron beam lithography and etched in an inductively coupled-plasma (ICP) reactive-ion etcher (RIE). Each waveguide contained a 2D random array of air holes that scattered light. The air hole diameters were 100 nm and the average (center-to-center) distance of adjacent holes was 390 nm. The waveguide walls were made of photonic crystals (triangle lattice of air holes, the lattice constant = 440 nm, the hole radius = 154 nm) that had a complete 2D band gap for in-plane confinement of light. However, light was scattered out of plane, and this leakage allowed us to observe light transport inside the disordered waveguide from the vertical direction.

The monochromatic light from a tunable cw laser source (HP 8168F) was coupled by an objective lens of numerical aperture (NA) = 0.4 into the empty waveguide. To ensure efficient confinement inside the waveguide, the light was

*yamilov@mst.edu
†hui.cao@yale.edu

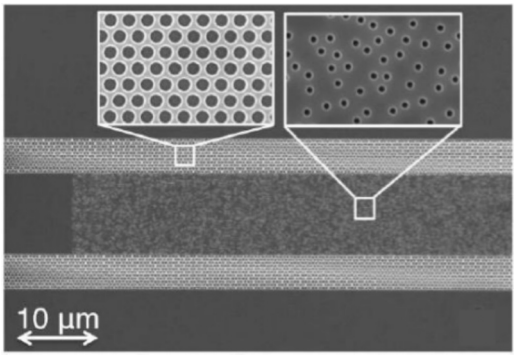

FIG. 1. Top-view scanning electron microscope (SEM) image of a quasi-2D disordered photonic waveguide. Light is injected from the left end of the empty waveguide and incident onto the random array of air holes. The waveguide wall is made of a triangle lattice of air holes which forms a 2D photonic band gap to confine light inside the waveguide.

transverse-electric (TE) polarized (electric field in the plane of the waveguide). The light was subsequently incident onto the random array of air holes inside the waveguide and underwent multiple scattering [Fig. 2(a)]. The near-field optical image of the spatial distribution of light intensity across the structure was taken by collecting light scattered out of plane using a 50× objective lens (NA = 0.42) and recorded by an InGaAs camera (Xeva 1.7-320). The spatial resolution was limited by the NA of the objective lens, and estimated to be ∼2 μm. Figure 2(b) is a typical near-field image, which exhibits short-range intensity fluctuations.

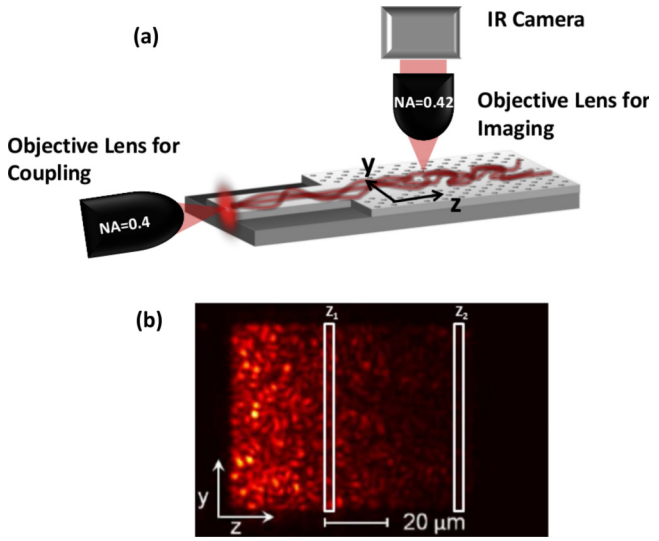

FIG. 2. (Color online) (a) A schematic of the optical measurement setup. One objective lens (NA = 0.4) couples the light from a tunable laser source to the waveguide, and another objective lens (50×, NA = 0.42) collects the light scattered by the air holes out of the waveguide plane and images onto a camera. (b) A near-field optical image of the intensity of scattered light from the disordered waveguide. The wavelength of the probe light is 1510 nm. The intensity distribution exhibits short-range fluctuations. z_1 and z_2 represent the axial positions of two cross sections inside the disordered waveguide.

The 2D intensity distribution inside the waveguide $I(y,z)$ was extracted from the near-field image [Fig. 2(b)]. $I(y,z)$ was then integrated along the cross section of the waveguide (y direction) to give the variation along the waveguide axis (z direction) $I(z)$. The spatial intensity correlation $\tilde{C}(z_1,z_2)$ was then computed from $I(z)$ as

$$\tilde{C}(z_1,z_2) = \frac{\langle I(z_1)I(z_2)\rangle}{\langle I(z_1)\rangle\langle I(z_2)\rangle} - 1, \quad (1)$$

where $\langle\cdots\rangle$ represents an ensemble average. $\tilde{C}(z_1,z_2)$ was measured for various combinations of z_1 and z_2 inside the disordered waveguides. The ensemble averaging was done over ten random configurations of air holes and 25 input wavelengths equally spaced between 1500 and 1510 nm. The wavelength spacing was chosen to produce different intensity distributions. Further averaging was done by generating different intensity distributions by slightly moving the input coupling spot along the transverse direction y. Nevertheless, since long-range correlation depends on the size and shape of the input beam [22], we ensured that the random array of air holes was illuminated uniformly along the y direction, so that diffusion occurs only along the z direction.

The relevant parameters for light propagation in the disordered waveguide are the transport mean free path ℓ and the diffusive dissipation length ξ_a. The transport mean free path ℓ depends on the size and density of the air holes. The dissipation mostly comes from out-of-plane scattering since the silicon absorption at the probe wavelength is negligible. As shown in our previous work [17], this vertical leakage of light can be treated as absorption and described by the diffusive dissipation length $\xi_a = \sqrt{D\tau_a}$, where τ_a is the ballistic absorption time and D is the diffusion coefficient For the disordered waveguides in Fig. 1, we found $\xi_a = 30\,\mu$m and $\ell = 2.2\,\mu$m by fitting the measured $I(z)$ with the diffusion equation. A detailed description of this procedure is given in Ref. [17]. The waveguide length is 80 μm, and the width varies from 10 to 60 μm. Thus the conductance g is between 1.6 and 9.9.

III. THEORY OF LONG-RANGE INTENSITY CORRELATION

Spatial intensity correlation defined by Eq. (1) involve intensities integrated over the cross section of the waveguide. Such integration suppresses the contribution from the short-range correlation C_1 so that only C_2 and C_3 remain. At the output end of the disordered waveguide ($z_1 = z_2 = L$), these two contributions reduce to the normalized variance of total transmission and the normalized variance of conductance, respectively [5,14]. C_2 and C_3 in lossy systems, such as those in our experiment, have been investigated before [7,23]. Although the expressions for C_2 and C_3 in Refs. [7,23] have been derived for diffusive samples ($g > 1$), they have been shown to also apply to the localized samples ($g \leqslant 1$) [24]. For the disordered waveguides in our experiment, C_2 is much larger than C_3. Thus we ignore C_3 and assume $\tilde{C} \simeq C_2$.

Next we obtain an expression for $C_2(z_1,z_2)$ which can be compared to the spatial correlation function defined in Eq. (1).

Such an expression has been derived using the Langevin approach in Refs. [10,25–27]. For a waveguide geometry we obtain

$$C_2(z_1,z_2) = \frac{2}{gL}\frac{\int_0^L \frac{\partial K(z_1,z')}{\partial z'}\frac{\partial K(z_2,z')}{\partial z'}\langle I(z')\rangle^2 dz'}{\langle I(z_1)\rangle\langle I(z_2)\rangle}, \quad (2)$$

where $K(z,z')$ is the solution of

$$\frac{\partial^2 K(z,z')}{\partial z^2} - \frac{K(z,z')}{\xi_a^2} = -\delta(z-z'), \quad (3)$$

with boundary conditions $K(0,z') = K(L,z') = 0$. Such a boundary condition neglects surface effects which can also lead to additional terms in Eq. (2). They are significant at $0 < z \lesssim \ell$, $L-\ell \lesssim z < L$ [27], particularly for the large index mismatch between inside and outside of the random medium. However, in our system of air holes in the dielectric, the effective refractive index of the random medium is less than that outside. In this case surface reflections are not pronounced [3]. Hence our choice of boundary conditions is reasonable for our samples with $\ell \ll L$.

The solution to Eq. (3) is

$$K(z,z') = \frac{\sinh\zeta_< \sinh(\mathcal{L}-\zeta_>)}{\xi_a^{-1}\sinh\mathcal{L}}, \quad (4)$$

where $\mathcal{L} = L/\xi_a$, $\zeta_< = \min[z,z']/\xi_a$, and $\zeta_> = \max[z,z']/\xi_a$. In the same approximation, $\langle I(z)\rangle \propto \sinh(\mathcal{L}-\zeta)/\sinh\mathcal{L}$. Substituting this expression as well as Eq. (4) into Eq. (2) we get $C_2(z_1,z_2)$. The final expression is cumbersome in the presence of loss, so we only list several limiting cases.

Case 1: Vanishing loss. In this case we take the limit $\xi_a \to \infty$ and get

$$C_2(z_1,z_2) = \frac{2z_1}{3gL^2}\frac{(2L-z_1)(L-z_1)+(L-z_2)^2}{L-z_1}, \quad (5)$$

which reduces to a well known result $C_2(L,L) = 2/3g$ at the output end.

Case 2: $z_2 = L$. This corresponds to correlating the intensity at the output surface with an intensity inside random medium. We get

$$C_2(z_1,L) = \frac{-8\zeta_1 + 4\zeta_1\cosh 2\mathcal{L} + 3(\sinh 2\mathcal{L} - \sinh 2\zeta_1) - 3\sinh 2(\mathcal{L}-\zeta_1) + 4(\mathcal{L}-\zeta_1)\cosh\mathcal{L}\,\mathrm{csch}(\mathcal{L}-\zeta_1)\sinh\zeta_1}{16g\mathcal{L}\sinh^2\mathcal{L}}, \quad (6)$$

where $\zeta_1 = z_1/\xi_a$. In a lossless random medium the above expression reduces to $C_2(z_1,L) = 2(2L-z_1)z_1/(g\ L^2)$, in agreement with the expression in Refs. [25,28].

Case 3: $z_1 = z_2 \equiv z$. Under this condition we obtain the normalized variance of the cross-section integrated intensity inside the waveguide,

$$\begin{aligned} C_2(z,z) = \{&4\zeta\cosh 2\mathcal{L} + 5\sinh 2\mathcal{L} \\ &- \sinh 2(\mathcal{L}-2\zeta) + \mathrm{csch}^2(\mathcal{L}-\zeta)[-4(\mathcal{L}-\zeta) \\ &+ \sinh 4(\mathcal{L}-\zeta)]\sinh^2\zeta - 4[2\zeta + \sinh 2(\mathcal{L}-\zeta) \\ &+ \sinh 2\zeta]\}[16g\mathcal{L}\sinh^2\mathcal{L}]. \end{aligned} \quad (7)$$

In the limit $z = L$ this quantity reduces to the normalized variance of the total transmission. In lossless medium Eq. (7) reduces to a compact expression $C_2(z,z) = (2z/gL)(1-2z/3L)$. We note that this function takes the maximum value $(9/8)C_2(L,L)$ at $z = 3L/4$, for any L.

In the following section we will compare the above theoretical predictions to the experimental data obtained for 2D disordered waveguides. Because of their reduced dimensionality, the waveguides are always localized in the $L \to \infty$ limit. The extent of the localization effects can be controlled by varying the ratio between system length L and the localization length $\xi = (\pi/2)N\ell$. Since N scales linearly with W, ξ can be easily tuned by varying the waveguide width without changing the transport mean free path and, hence, maintaining constant diffusive absorption length ξ_a. Therefore, by changing the waveguide geometry (e.g., L or W), we can reach both the diffusion regime ($\ell < L < \xi$) and the localization regime ($\xi < L$) [17]. In this work we concentrate on the diffusion regime. We note that, although there is no mobility edge in the waveguide geometry, it is not essential for our goal of observing the development of spatial correlation inside random media of finite size.

IV. EXPERIMENTAL RESULTS AND COMPARISON TO THEORY

Figure 3 shows the measured $\tilde{C}(z_1,z_2)$ for a disordered waveguide of $L = 80$ μm, $W = 60$ μm, $\xi_a = 30$ μm, and $\ell = 2.2$ μm. z_1 is varied between 0 and L while z_2 is fixed at L or $L/2$. As the distance between z_1 and z_2 increases, $\tilde{C}(z_1,z_2)$ decays gradually. Even when the distance becomes much larger than the transport mean free path, the intensity correlation does not vanish. The correlation builds up further into the sample. As shown in the inset of Fig. 3, for a fixed distance $\Delta z = z_2 - z_1 = 10$ μm, $\tilde{C}$ grows as z_2 moves from $L/4$ to L. The experimentally observed long-range correlation inside the random system agrees well with the theoretical predictions represented by the solid lines in Fig. 3.

Next we demonstrate the ability to manipulate the long-range correlation by adjusting the width W of the waveguide while keeping the length L and the degree of disorder the same. Figure 4 compares $\tilde{C}(z_1,z_2)$ for two disordered waveguides of length $L = 80$ μm and $W = 10$ and 60 μm. z_1 is moved from 0 and L while z_2 is set at L. The localization length ξ falls from 788 μm for $W = 60$ μm to 131 μm for $W = 10$ μm. Hence, the former is in the diffusion regime ($\ell \ll L \ll \xi$), while the latter approaches the localization regime ($L \sim \xi$). The conductance g, which is proportional to W, drops by a factor of 6 from 9.85 to 1.64. The probability for two scattering paths crossing, which scales as $1/g$, is thus enhanced by a factor of 6. This leads to a sixfold increase of the long-range intensity correlation, as indeed observed experimentally and

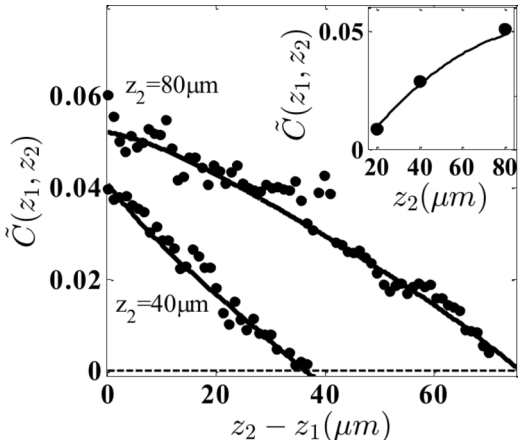

FIG. 3. Long-range intensity correlation $\tilde{C}(z_1,z_2)$ in a disordered waveguide of $L = 80$ μm, $W = 60$ μm, $\xi_a = 30$ μm, and $\ell = 2.2$ μm. z_1 is varied between 0 and L while z_2 is fixed at L or $L/2$. Solid circles are experimental data and solid lines represent the theoretical predictions of Eqs. (2) and (6). The dashed line corresponds to the background taken outside the waveguide. The inset shows $\tilde{C}(z_1,z_2)$ for $\Delta z = z_2 - z_1 = 10$ μm and $z_2 = L, L/2, L/4$. Solid circles are experimental data and the solid line represents the theoretical prediction of Eq. (2). For a fixed Δz, $\tilde{C}(z_1,z_2)$ increases when moving deeper into the sample.

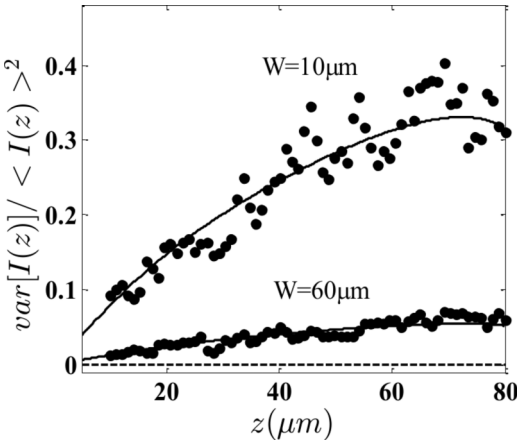

FIG. 5. Normalized variance of the cross-section integrated intensity $I(z)$, $\mathrm{var}[I(z)]/\langle I(z)\rangle^2$, for two waveguides with the same length $L = 80$ μm and degree of disorder ($k\ell = 26$) but different widths $W = 60$ and 10 μm. z is changed from 0 to L. The solid circles are experimental data and solid lines represent the theoretical predictions of Eq. (7). The dashed line corresponds to the background taken outside the waveguide. The six-times reduction of the waveguide width results in a sixfold increase in the magnitude of the intensity fluctuations.

in agreement with the theory in Sec. III. We note that the enhancement of long-range correlation is caused purely by the change of waveguide geometry with no modification of the scattering strength.

Finally, we measured the variance of the cross-section-integrated intensity $I(z)$ inside the disordered waveguides. As mentioned above, the normalized variance, $\mathrm{var}[I(z)]/\langle I(z)\rangle^2 = \tilde{C}(z_1 = z, z_2 = z)$, becomes equal to the normalized variance of total transmission when $z = L$.

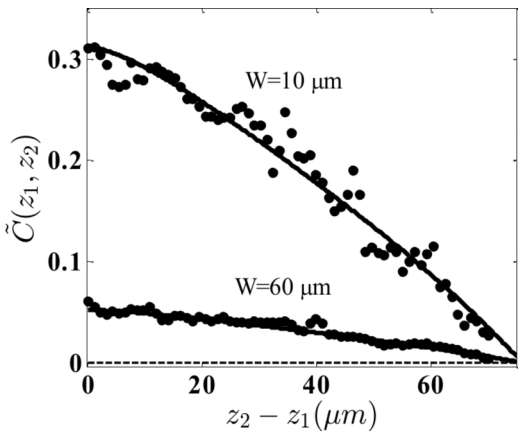

FIG. 4. Long-range intensity correlation $\tilde{C}(z_1,z_2)$ for two waveguides with the same length $L = 80$ μm and the degree of disorder ($k\ell = 26$) but different widths $W = 60$ and 10 μm. z_1 is moved from 0 to L and z_2 is set at L. Solid circles are experimental data and solid lines represent the theoretical predictions of Eq. (6). The dashed line corresponds to the background taken outside the waveguide. The six-times reduction of the waveguide width results in a sixfold increase in the magnitude of the intensity correlation.

Figure 5 shows the measured variance inside two disordered waveguides of width $W = 10$ and 60 μm. The other parameters are the same as in Fig. 4. z is changed from 0 to L. The fluctuations of $I(z)$ grow with the depth of the random system. In a narrower waveguide, the fluctuation is larger due to the more pronounced localization effect (smaller conductance).

V. CONCLUSION

In summary, we directly measured the long-range spatial intensity correlation inside the quasi-two-dimensional disordered waveguides. Light scattered out of the waveguide plane allowed us to probe the internal transport from the third dimension. The long-range intensity correlation gradually builds up as light propagates through the random system. The fluctuations of cross-section integrated intensity also grow with the depth into the disordered waveguide. Good agreements between experiment and theory are obtained. By reducing the waveguide width, we are able to enhance the long-range intensity correlation and the relative intensity fluctuations, without modifying the degree of disorder. This provides an approach for the manipulation of long-range spatial correlation of light intensity inside random media.

ACKNOWLEDGMENTS

We acknowledge Douglas Stone and Arthur Goetschy for valuable discussions. We also thank Michael Rooks for useful suggestions on sample fabrication. This work was supported by the National Science Foundation under Grants No. DMR-1205307, No. DMR-1205223, No. ECCS-1128542, and No. ECCS-1068642. Facilities used were supported by YINQE and NSF MRSEC Grant No. DMR-1119826.

[1] *Scattering and Localization of Classical Waves in Random Media*, edited by P. Sheng (World Scientific, Singapore, 1990).
[2] R. Berkovits and S. Feng, Phys. Rep. **238**, 135 (1994).
[3] M. C. van Rossum and T. M. Nieuwenhuizen, Rev. Mod. Phys. **71**, 313 (1999).
[4] P. Sheng, *Introduction to Wave Scattering, Localization, and Mesoscopic Phenomena* (Academic, Boston, 1995).
[5] E. Akkermans and G. Montambaux, *Mesoscopic Physics of Electrons and Photons* (Cambridge University Press, Cambridge, UK, 2007).
[6] M. J. Stephen and G. Cwilich, Phys. Rev. Lett. **59**, 285 (1987).
[7] R. Pnini, in *Proceedings of the International Physics School on Waves and Imaging Through Complex Media*, edited by P. Sebbah (Kluwer Academic, Dordrecht, 2001), p. 389.
[8] A. Z. Genack, N. Garcia, and W. Polkosnik, Phys. Rev. Lett. **65**, 2129 (1990).
[9] M. P. van Albada, J. F. de Boer, and A. Lagendijk, Phys. Rev. Lett. **64**, 2787 (1990).
[10] J. F. de Boer, M. P. van Albada, and A. Lagendijk, Phys. Rev. B **45**, 658 (1992).
[11] N. Garcia, A. Z. Genack, R. Pnini, and B. Shapiro, Phys. Lett. A **176**, 458 (1993).
[12] F. Scheffold, W. Härtl, G. Maret, and E. Matijević, Phys. Rev. B **56**, 10942 (1997).
[13] P. Sebbah, R. Pnini, and A. Z. Genack, Phys. Rev. E **62**, 7348 (2000).
[14] P. Sebbah, B. Hu, A. Z. Genack, R. Pnini, and B. Shapiro, Phys. Rev. Lett. **88**, 123901 (2002).
[15] A. A. Chabanov, N. P. Trégourès, B. A. van Tiggelen, and A. Z. Genack, Phys. Rev. Lett. **92**, 173901 (2004).
[16] O. L. Muskens, T. van der Beek, and A. Lagendijk, Phys. Rev. B **84**, 035106 (2011).
[17] A. G. Yamilov, R. Sarma, B. Redding, B. Payne, H. Noh, and H. Cao, Phys. Rev. Lett. **112**, 023904 (2014).
[18] S. Feng, C. Kane, P. A. Lee, and A. D. Stone, Phys. Rev. Lett. **61**, 834 (1988).
[19] S. Feng and P. A. Lee, Science **251**, 633 (1991).
[20] F. Scheffold and G. Maret, Phys. Rev. Lett. **81**, 5800 (1998).
[21] C. P. Lapointe, P. Zakharov, F. Enderli, T. Feurer, S. E. Skipetrov, and F. Scheffold, Europhys. Lett. **105**, 34002 (2014).
[22] R. Pnini and B. Shapiro, Phys. Rev. B **39**, 6986 (1989).
[23] P. W. Brouwer, Phys. Rev. B **57**, 10526 (1998).
[24] A. Yamilov and H. Cao, Phys. Rev. E **70**, 037603 (2004).
[25] R. Pnini and B. Shapiro, Phys. Lett. A **157**, 265 (1991).
[26] A. A. Lisyansky and D. Livdan, Phys. Lett. A **170**, 53 (1992).
[27] A. A. Lisyansky and D. Livdan, Phys. Rev. B **47**, 14157 (1993).
[28] E. Kogan and M. Kaveh, Phys. Rev. B **45**, 1049 (1992).